DOI: 10.1016/j.jeurceramsoc.2014.08.028

Thickness-dependence of the breakdown strength: Analysis of the dielectric and mechanical failure

C. Neusel[a], H. Jelitto[a], D. Schmidt[a], R. Janssen[a], F. Felten[b], G. A. Schneider[a,*]

[a]Hamburg University of Technology, Institute of Advanced Ceramics, Denickestr. 15, 21073 Hamburg, Germany

[b]Robert Bosch GmbH, Corporate Research and Advance Engineering, Advanced Functional and Sintered Materials, 70049 Stuttgart, Germany

*Corresponding author: Gerold A. Schneider
E-Mail: g.schneider@tuhh.de.de
Tel: +49-(0)40 42878 3037
Fax: +49-(0)40 42878 2647

Abstract

The breakdown strength as well as the mechanical strength of ceramic materials decreases with increasing volume. The volume-effect of the mechanical strength can be explained by the Weibull theory. For the breakdown strength the same explanation has been often assumed. In order to validate this assumption breakdown strength and mechanical strength of alumina samples with defined porosities were compared. Differences in the Weibull moduli of breakdown and mechanical strength distributions indicate that the volume-effect cannot explain the thickness-dependence of the breakdown strength. In particular, the thickness-dependence of the breakdown strength always leads to a Weibull modulus of two which is not

in agreement with the measured Weibull moduli for samples with constant thickness. It can be concluded that the thickness-dependence of the breakdown strength cannot be explained by the Weibull concept. A recently developed breakdown model which is based on space charge injection is able to explain the experimental results.

Keywords: Breakdown strength; thickness-dependence; Weibull modulus; fracture strength; volume-effect;

1. Introduction

In applications, ceramics are interesting due to their good electrical insulation properties even at high temperatures. Insulators electrically fail when a dielectric breakdown event happens, which leads to a formation of an electrically conductive channel through the insulator. It is assumed that the initiation of breakdown happens, due to a sudden destabilization of trapped charges [1-3], which causes a current flow through the material. The breakdown strength, E_b, defined as breakdown voltage, V_b, per sample thickness, t, is reported to be dependent on the microstructure [2-4], sample thickness [5-9] and loading condition [8, 10-12]. The influence of the porosity [2, 13-15], grain size [2-4, 13, 15-17], purity and secondary phase [2-4, 6, 7] on the breakdown strength have been investigated. However, no suitable holistic model has been developed, explaining the experimental results.

The thickness-dependence of the breakdown strength ($E_b \propto t^{-\frac{1}{2}}$) has been often explained as volume-effect similar to the mechanical case [5, 18, 19].

Mechanical failure of ceramic materials occurs due to microstructural defects. The fracture strength of ceramics shows due to the volume-effect a thickness-dependence, as the probability for a large fracture initiating defect increases with increasing sample thickness and thus its volume [20]. Hence, it was suggested that there is a correlation between electrical and

mechanical failure. For hardened gypsum, $BaTiO_3$- and TiO_2-ceramics the mechanical strength distributions of three- respectively four-point-bending tests and the breakdown strength distributions were evaluated [21-24]. By comparing the mechanical and dielectric Weibull moduli, an analogy between mechanical and dielectric strength distribution was found, whereas Young et al. [25] could not confirm this result based on experiments with $BaTiO_3$ multilayer-capacitors.

A model, which combines electrical and mechanical parameters, is the electromechanical breakdown model originally proposed by Stark and Garton [26] for polymers. This model was further developed by Zeller et al. [27] and Fothergill [28], who introduced, in analogy to fracture mechanics, a Griffith criterion for the growth of a partial discharge channel into the dielectric. The filamentary electromechanical breakdown model, proposed by Fothergill, is in good agreement with experimental results of polymers. But for ceramic materials, it has been shown by Carabajar et al. [29] that there is no good correlation with experimental results. However, if the thickness-dependence could be explained by a volume-effect, a similar dependence would have been measurable when keeping the thickness constant and varying the testing area [12]. This hypothesis could not be confirmed by experiments [30, 31].

The aim of this paper is to compare Weibull moduli of dielectric breakdown tests with Weibull moduli of mechanical “Punch on three Balls” (P3B) tests of alumina samples with defined porosities. The advantage of the P3B-test is that disc-shaped alumina samples can be used with the same geometry as for the electric breakdown test. Additionally, the P3B-test results show high robustness with respect to slight deviations from the ideal sample geometry [32, 33]. Using identical processed samples with same geometry for both the electrical and mechanical tests eliminates influences from microstructure and surface finishing. The samples under investigation have defined porosities from 2 to 8 vol-%. Assuming that the failure initiating defects for the mechanical and also for the electrical test are identical, the resulting Weibull moduli should be equal within the confidence interval. Furthermore, Weibull moduli

of breakdown experiments on alumina samples with increasing thickness (0.3 – 1.5 mm) were evaluated. If the thickness-dependence of the breakdown strength were due to a volume-effect, a Weibull modulus of two would be expected, as according to the volume-effect the slope of the double-logarithmic E_b - t - curve equals the inverse Weibull modulus.

2. Materials and methods

2.1 Sample preparation

Dielectric breakdown tests and mechanical P3B-tests were performed on cylindrical polycrystalline Al_2O_3 samples with adjusted porosity.

As alumina base powder Taimicron TM-DAR (Krahn Chemie GmbH, Germany) with a purity of 99.99% and a mean particle size of 0.2 µm was used for sample processing. In order to reach a defined porosity, rice starch as pore builder was taken. The rice starch was sieved with 25µm and mixed with the Al_2O_3 base powder via speed mixer (DAC 150 FVZ, Hausschild, Germany) at 2500 rpm for 1 min. Depending on the porosity that should be reached in the sintered sample different amounts of rice starch were mixed with the alumina base powder. With the aim of reaching 2.5, 5 and 7.5 vol-% porosity in the sintered sample, 1, 2 and 3 g rice starch were mixed with the alumina base powder, to a total amount of 100 g mixed-powder. After speed mixing, the powder was sieved with 355 µm for homogenization. In the following, alumina samples without rice starch are labelled as AO-R0, the samples with 1, 2 and 3 g rice starch are labelled as AO-R1, AO-R2, and AO-R3.

From these powder mixtures, samples with a diameter of 28 mm were prepared by sequential uniaxial dry pressing at 8.2 and then 17 MPa with the uniaxial press (Uniaxialpresse, Paul Weber GmbH, Germany). This process was followed by cold-isostatic dry pressing (KIPP200ES, Paul Weber GmbH, Germany) at 150 MPa. After pressing, the samples were sintered in a chamber furnace (HT 04/17 Naber, Germany) in air. The sintering cycles for the

powders with and without rice starch can be found in table 1. The sintering cycle for the powder with rice starch differs from powder without rice starch in the first step. For the powder with rice starch the temperature was increased with 5 K/min up to 700°C, followed by a holding time of 1h, in order to burn out the rice starch.

After sintering, the samples were ground plan-parallel to a thickness of 1.0 mm with a flat-bed grinding machine (Blohm HFD 204, Hauni, Germany). In order to proof the known thickness-dependence of the breakdown strength [5-9] alumina samples without rice starch AO-R0 were ground to thicknesses of 0.3, 0.5, 1.0 and 1.5 mm. Alumina samples with rice starch AO-R2 were ground to thicknesses of 0.5 and 1.0 mm.

Table 1: Sintering cycle for the alumina powder with and without rice starch.

Sample	**Sintering cycle**
Al_2O_3 without rice starch, AO-R0	10 K/min to 1350°C for 1 h 10 K/min to 40°C
Al_2O_3 with rice starch, AO-R1, AO-R2, AO-R3	5 K/min to 700°C for 1h, 10 K/min to 1350°C for 1 h 10 K/min to 40°C

2.2 Sample characterization

After polishing and thermal etching, the grain size of the samples was characterized according to the mean intercept length method. The density was evaluated with the Archimedes method. Based on light microscope images from the polished surface the porosity and pore size were analysed using an optical method via the software ImageJ (developed by W. Rasband, National Institute of Health, USA).

2.3 Dielectric breakdown test

The dielectric breakdown tests were performed using a rectified AC voltage signal as described by Neusel et al. [34]. The voltage signal was realized by a 50 Hz voltage pulse, generated by a function generator (Agilent 33220 A, Agilent Technologies, USA), which was stepwise amplified by vacuum tubes, inductors and a transformer coil from low to high voltage.

The tests were performed in a measurement cell, which mainly consists of a brass-made pin electrode as high-voltage electrode and a ground-electrode made of stainless steel. The high-voltage electrode was enclosed by PVC-cylinder to prevent flash-over behaviour from the high-voltage to the ground-electrode. The ground-electrode has a flat surface area with rounded edges, similar to a Rogowski profile. Besides the pulsed voltage signal a DC voltage signal was used to test 0.3 and 1.0 mm thick samples. The 0.3 mm thick samples were tested with a DC high voltage generator HCN 140-35000 (F.u.G. Elektronik GmbH, Germany) which can create a maximum voltage of 35 kV. The 1.0 mm samples were tested with a DC high voltage generator ER75P4 (Glassman high voltage Inc., UK), which can generate a maximum voltage signal of 75 kV.

Before dielectric breakdown testing, a circular shaped layer of conductive silver paste with a diameter of 10 mm was applied onto the sample surface, to ensure a good connection between sample and attaching electrodes. For the evaporation of the paste's solvent, the samples were placed in a cabinet dryer (Heraeus T 5050E, Heraeus Holding, Germany) at 100°C for 5 h before testing.

The breakdown tests were performed in silicon oil at room temperature. Therefore, the samples were placed into the measurement cell between high-voltage and ground-electrode. The voltage signal was amplified with a rate of 0.2 kV/s, until the sample underwent dielectric breakdown, characterized by a collapsing of the voltage signal and in most cases accompanied by a light and noise emission.

2.3 Mechanical strength-test

The mechanical tests were conducted with the universal testing machine (series 1600, ATS, USA) using the method “Punch on three Balls” (P3B). The P3B-method enables to perform flexural strength testing of brittle disc-shaped samples. The test assembly was built up of a guide-ring, which ensures a threefold symmetrical adjustment of the three metal bearing balls. The disc-shaped sample was centrally arranged onto these thee bearing balls, so that the sample was supported on three points near its periphery. The metal punch was a ball with a flat surface area to ensure a stable positioning centrically on the opposite sample surface (fig.1). With the load frame of the universal testing machine a constant axial load was transferred via punch central onto the sample surface until the sample fractures. The maximum load was measured during the testing procedure. The fracture strength σ_{max} is calculated according to the following equation [35]

$$\sigma_{max} = \frac{3F}{4\pi t^2}\left[\frac{(1-\nu)(2r^2 - r_0^2)}{2R^2} + 2(1+\nu)\ln\frac{r}{r_0} + (1+\nu)\right] \quad (1)$$

with the maximum load F, sample thickness t and sample radius R, ν the Poisson ratio of alumina with 0.23 [20], r the radius of the bearing balls with 10 mm and r_0 the contact radius of the upper punch being 2.89 mm.

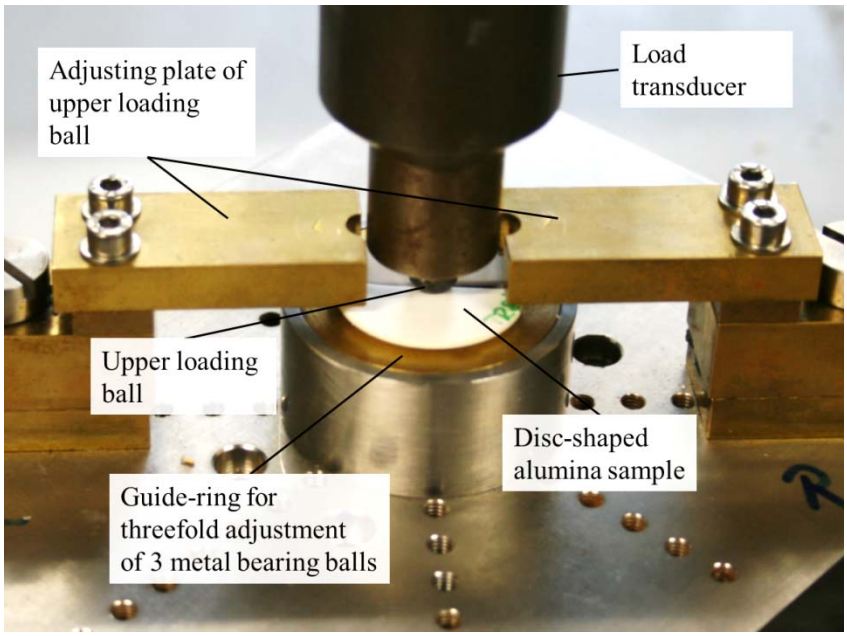

Fig. 1: Test set-up of mechanical test "Punch on three Balls" with mounted alumina sample.

With the P3B-setup 1.5 mm thick AO-R0 and 1.0 mm thick AO-R1, AO-R2 and AO-R3 samples were tested.

3. Calculation

In the following section the volume-effect of the mechanical strength and the breakdown strength distribution will be derived based on the Weibull theory. At the end of this section a constant ratio of the mechanical and electrical Weibull modulus is derived. If the thickness-dependence of the breakdown strength was due to a volume-effect, this constant ratio should be measured experimentally.

For brittle materials like ceramics it has been shown that the mean number of critical defects N_c^m in a volume V under a uniaxial mechanical stress σ_c leads to a failure probability for mechanical failure [20, 36-40]:

$$P_f^m = 1 - \exp\left[-N_c^m(\sigma_c, V)\right] \qquad (2)$$

A critical defect is defined as a defect of length a_c where the fracture criterion is fulfilled when a critical mechanical stress σ_c is applied [20, 36-40]:

$$G_m(a_c, \sigma_c, Y) = G_c^m \qquad (3)$$

where G_c^m is the toughness, G_m the mechanical energy release rate and Y the Young's modulus of the material. The mechanical energy release rate for small defects in the volume of a ceramic is:

$$G_m(a_c, \sigma_c, Y) = \frac{\sigma_c^2 \pi a_c f(\textit{defect shape}, \textit{location})}{Y} \qquad (4)$$

where the function f(*defect shape, location*) is the so-called geometry factor of the defect which depends on its shape and location within the component. Assuming brittle materials, a relation between the Pareto distribution, describing the crack size frequency density, and the Weibull distribution can be derived [37]. It is assumed that the length of defects a in a ceramic is statistically distributed with the following frequency per volume:

$$g(a) = \frac{r-1}{V_0 a_0}\left(\frac{a}{a_0}\right)^{-r}, \ (r > 1) \tag{5}$$

where r is a constant, V_0 is a normalization volume and a_0 a normalization defect length. Hence, the mean number of critical defects in a volume V is:

$$N_c^m(a_c, V) = V\int_{a_c}^{\infty} g(a)da = \frac{V}{V_0}\left(\frac{a_c}{a_0}\right)^{1-r} \tag{6}$$

Applying (4) to replace a_c and a_0 in (6) gives

$$N_c^m(\sigma_c, V) = \frac{V}{V_0}\left(\frac{\sigma_c}{\sigma_0}\right)^{2(r-1)} \tag{7}$$

and leads to the Weibull distribution for the failure probability of brittle materials [20, 36-40]

$$P_f^m = 1 - \exp\left[-\frac{V}{V_0}\left(\frac{\sigma_c}{\sigma_0}\right)^m\right] \tag{8}$$

with the Weibull modulus m:

$$m = 2(r-1) \tag{9}$$

and σ_0 is defined as:

$$\sigma_0 \equiv \left(\frac{G_c^m Y}{\pi a_0 \, f(\text{defect shape}, \text{location})}\right)^{\frac{1}{2}} \tag{10}$$

Throughout the calculations it is assumed that f (*defect shape, location*) is constant for all the defects of the distribution.

Based on equation 8 the correlation of the mechanical fracture strength, σ_{c1} and σ_{c2} to the volume, V_1 and V_2, can be described as [20, 36-40]

$$\frac{\sigma_{c1}}{\sigma_{c2}} = \left(\frac{V_2}{V_1}\right)^{\frac{1}{m}} \tag{11}$$

This well-known approach to explain the mechanical Weibull distribution is now generalized to derive a failure probability for the dielectric breakdown strength. It is assumed that the

same defect population triggers the mechanical and dielectric breakdown. But for the dielectric breakdown a specific "fracture criterion" is necessary which is called the dielectric breakdown criterion. Further, it is assumed that also an energy release rate based criterion is valid and that an electrical energy release rate G_b exists which depends on the applied breakdown field E_b, the critical defect length a_c and the permittivity ε as follows:

$$G_b(a_c, E_b, \varepsilon) = E_b^{\alpha} a_c^{\beta} \varepsilon^{\gamma} h(\textit{defect shape}, \textit{location}) \qquad (12)$$

α, β and γ are constants and h (*defect shape, location*) is a function similar to the geometry factor for the mechanical case. It is assumed that if this dielectric energy release rate reaches a critical value G_c^{bd} unstable dielectric breakdown will happen. Therefore, the dielectric breakdown criterion is:

$$G_b(a_c, E_b, \varepsilon) = G_c^{bd} \qquad (13)$$

Analogous to (2) the failure probability for dielectric failure is:

$$P_f^{bd} = 1 - \exp\left[-N_c^{bd}(E_b, V)\right] \qquad (14)$$

with the proposed dielectric energy release rate (12) the critical defect size can be calculated together with (13) and introduced into (6). The result is:

$$N_c^{bd}(E_b, V) = \frac{V}{V_0}\left(\frac{E_b}{E_0}\right)^{\frac{\alpha}{\beta}(r-1)} \qquad (15)$$

and it follows for the failure probability of the dielectric breakdown strength:

$$P_f^{bd} = 1 - \exp\left[-\frac{V}{V_0}\left(\frac{E_b}{E_0}\right)^{m_{bd}}\right] \qquad (16)$$

with the breakdown Weibull modulus m_{bd}:

$$m_{bd} = \frac{\alpha}{\beta}(r-1) \qquad (17)$$

Based on equation 16 the correlation of the breakdown strength, E_{b1} and E_{b2}, to the volume, V_1 and V_2, can be described as [31]

$$\frac{E_{b1}}{E_{b2}} = \left(\frac{V_2}{V_1}\right)^{\frac{1}{m_{bd}}} \qquad (18)$$

From the derivation of the breakdown and mechanical Weibull modulus (equ. 9, 17) it follows that their ratio should be constant ($\frac{m_{bd}}{m} = \frac{\alpha}{2\beta}$), if both the mechanical and dielectric failure originated from the same defect size distribution.

4. Results

4.1 Sample characterization

All samples, sintered with a sintering temperature of 1350 °C for 1 h, show a grain size of approximately 1 µm. The densities of the samples evaluated with the Archimedes method and the mean pore size with standard deviation are given in table 2. Alumina samples without rice starch reach a density of about 3.90 ± 0.04 g/cm³, which means a porosity of 1.8 vol-%, according to the supplier's given theoretical density of 3.97 g/cm³. The addition of 1, 2 and 3 g rice starch to the alumina powder led to a porosity of 4.0, 6.3 and 7.6 vol-%.

In figure 2 the light microscope images of the samples with different porosities are shown. From these images the mean and maximum pore diameter were evaluated using the software ImageJ. The mean pore diameter of samples with rice starch as pore builder is approximately 7.3 µm, the maximum pore diameter in the range of 22 to 34 µm. Samples without rice starch show a mean pore diameter of approximately 4.4 µm and a maximum pore diameter of 13 µm.

Table 2: Density and porosity of the samples evaluated with the Archimedes method. The mean pore diameter with standard deviation was evaluated by the software ImageJ from light microscope images.

	Density ± ST.D. [g/cm³]	**Porosity [vol-%]**	**Mean pore diameter ± ST.D. [µm]**	**Max. pore size [µm]**
AO-R0	3.90 ± 0.04	1.8	4 ± 2	13
AO-R1	3.81 ± 0.06	4.0	7 ± 4	22
AO-R2	3.72 ± 0.06	6.3	8 ± 7	29
AO-R3	3.67 ± 0.04	7.6	7 ± 5	34

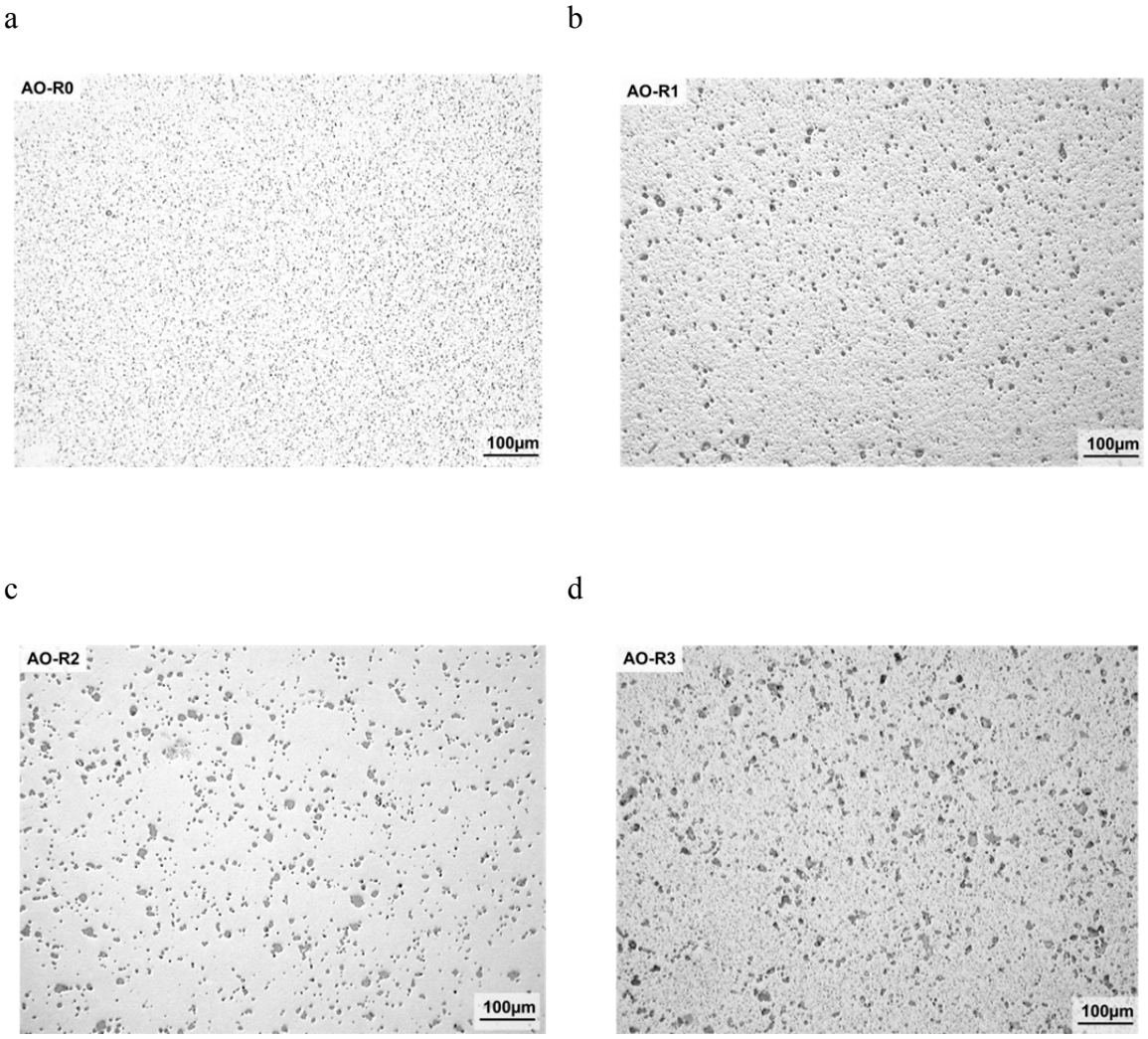

Fig. 2: Light-microscope images of a polished cross section of alumina samples a) AO-R0 with 0 wt-% rice starch, b) AO-R1 with 1 wt-% rice starch, c) AO-R2 with 2 wt-% rice starch and d) AO-R3 with 3 wt-% rice starch.

4.2 Mechanical strength-test

Weibull diagram of mechanical test

Mechanical fracture P3B-tests were done on samples AO-R0 without rice starch and AO-R1, AO-R2 and AO-R3 with rice starch as pore builder. All tested samples have a thickness of 1.0 mm except the AO-R0 samples which were 1.5 mm in thickness. Although the effective volume of AO-R0 will be larger compared to AO-R1, AO-R2 and AO-R3 which have the same effective volume it is assumed according to Danzer et al. [32] that the Weibull moduli will be comparable. For a better presentation of the results two Weibull diagrams of the P3B-test are given in figure 3a and b. The Weibull moduli, m_{P3B}, calculated according to the maximum likelihood method and the characteristic Weibull fracture strengths, σ_0, with 90% confidence intervals (CI) are evaluated according to DIN EN 843-5 [41] and summarized in table 3.

From literatures [42, 43] it is known that the fracture strength decreases with increasing porosity, assuming a constant pore size. The characteristic Weibull fracture strength, σ_0, of AO-R0 and AO-R1 are statistically equal, as the confidence intervals are overlapping (tab.3). Here, it must be taken into account, that the samples AO-R0 were tested with a thickness of 1.5 mm, whereas the thickness of AO-R1 was 1.0 mm. The consequence of the thicker samples AO-R0 is that the loaded effective volume is higher compared to 1 mm thick samples AO-R1, which result in a lower fracture strength as it were expected for AO-R0 tested with 1 mm thickness.

Further, AO-R2 samples show a σ_0 with 90%-CI of 273 [259; 289] MPa, which is lower compared to AO-R3 samples with a σ_0 and 90%-CI of 336 [322; 351] MPa.

a b

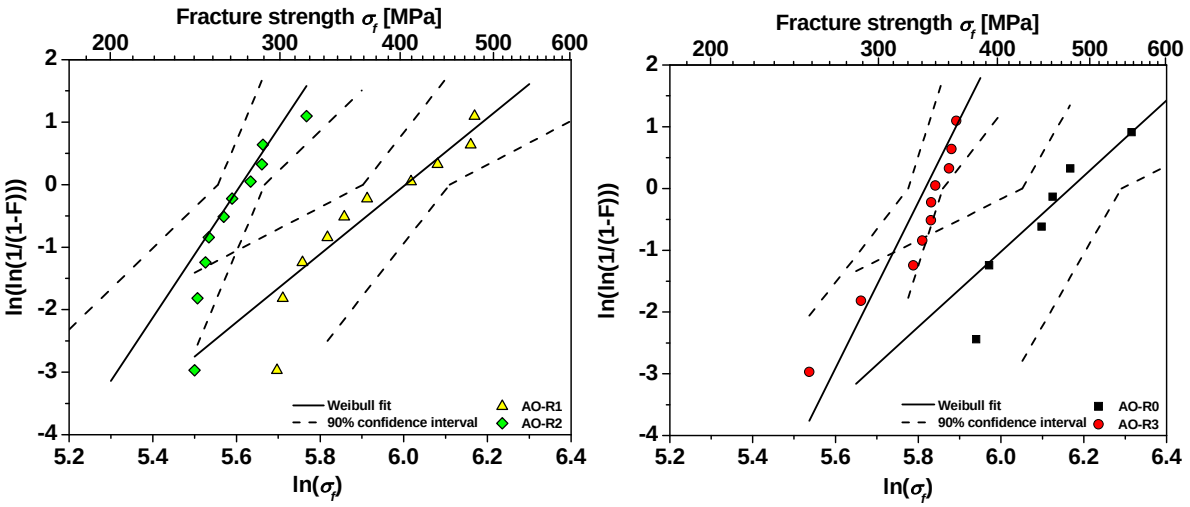

Fig. 3: Double logarithmic Weibull diagrams of the mechanical "Punch on three Balls"-test of alumina samples a) AO-R1 and AO-R2 with rice starch as pore builder (all 1.0 mm thick) and b) AO-R0 without rice starch as pore builder (1.5mm thick) and AO-R3 with rice starch as pore builder (1.0 mm thick). The black lines are Weibull fits and the dashed lines are 90% confidence intervals.

This unexpected lower fracture strength of the samples AO-R2, which are less porous compared to the samples AO-R3, can be explained by the microstructure. Figure 4 shows the microstructure of AO-R2, analyzed from AO-R2 samples which were used for the P3B-test. The mean pore diameter is 8 ± 7 µm and comparable to the samples AO-R3 (tab. 2). But the maximum pore diameter is 59 µm for AO-R2 compared to 34 µm for AO-R3. As mechanical fracture initiates at the biggest mechanically loaded defect of the sample, presumably the lager maximum pore size of AO-R2 samples used in the P3B-test caused lower fracture strength.

The larger maximum pore size of AO-R2 samples used in the P3B-test (fig. 4) compared to AO-R2 samples used in the breakdown test (fig. 2c) could be attributed to a missed step in the production process, namely the sieving of rice starch with 25µm or sieved rice starch was used which was agglomerated again due to the storage time.

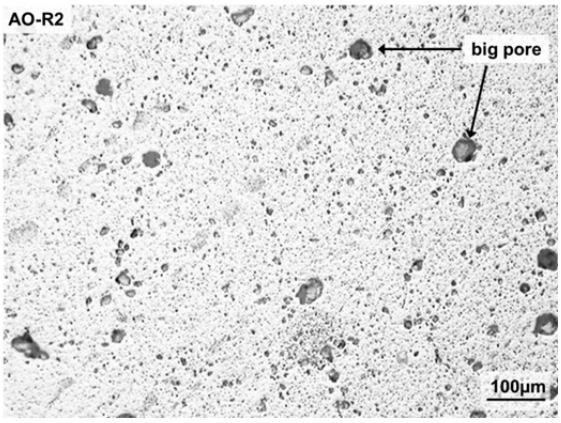

Fig. 4: Light-microscope image of the polished surface of AO-R2 sample after using it in the mechanical "Punch on three Balls"- test.

4.3 Dielectric breakdown test

In the following analysis, the breakdown strength E_b defined as ratio of the breakdown voltage V_b and the sample thickness t is used according to common practice [44]. Here, it should be mentioned that this definition does not account for field enhancements at, e.g. electrode edges. These effects can only be considered for known geometries by numerical methods as, e.g. shown by Block et al. [45].

Weibull analysis of porous samples

After the grinding process normally not all samples AO-RO, AO-R1, AO-R2 and AO-R3 have exactly the same thickness of 1.0 mm but vary up to 10 %. Therefore, the measured breakdown strengths, E_b, are normalized for each batch with respect to the corresponding sample thickness. The equation to calculate the normalized breakdown strength, E_{bn}, is as follows:

$$E_{bn} = \sqrt{\frac{t_m}{t}} E_{bm} \qquad (19)$$

with t_m as measured sample thickness after grinding, t the intended target thickness (here, 1.0 mm) and E_{bm} the measured breakdown strength. The normalization is calculated according to the dependence of the breakdown strength to the sample thickness which is approximately $E_b \propto t^{-\frac{1}{2}}$ for alumina [6-9, 46].

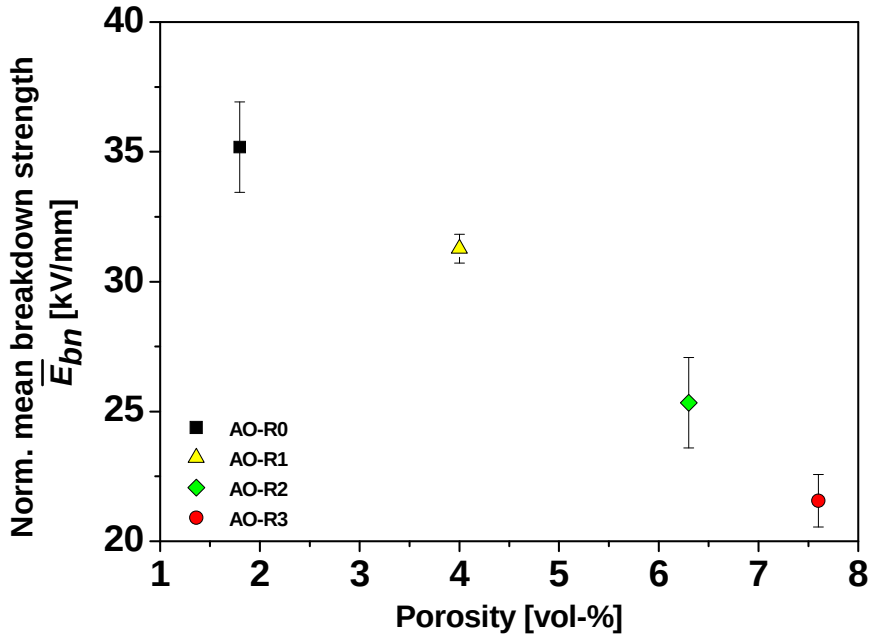

Fig. 5: Normalized mean breakdown strength $\overline{E}_{bn}$ with standard deviation as function of the porosity for alumina samples AO-R0, AO-R1, AO-R2 and AO-R3 (normalization thickness t = 1.0 mm).

In figure 5 the influence of the porosity on the mean breakdown strength is displayed. As expected from literatures [2, 13-15] the breakdown strength decreases with increasing porosity. But in contrast to Liebault et al. [2], who reported that a porosity of the sample below 5 vol-% has no effect on the breakdown strength, here, an effect of the porosity on the breakdown strength even below 5 vol-% can be shown. The $\overline{E}_{bn}$ with standard deviation (ST.D.) for AO-R0 samples is 35 ± 2 kV/mm, whereas $\overline{E}_{bn}$ ± ST.D. for AO-R1 samples is 31 ± 1 kV/mm. All measured and normalized breakdown strength data E_{bn} were analyzed according to a Weibull distribution and plotted in a Weibull diagram in figure 6. The Weibull

modulus for breakdown, m_{bd}, and the characteristic Weibull breakdown strength, $E_{0,}$ with 90% confidence intervals (CI) are evaluated in analogy to DIN EN 843-5 [41]. The equations to calculate the Weibull modulus for breakdown according to the maximum likelihood method based on DIN EN 843-5 [41] were reformulated as follows

$$\frac{1}{m} = \frac{\sum_{i=1}^{i=n}\left(\ln E_{bn}^{i} \cdot \left(E_{bn}^{i}\right)^{m}\right)}{\sum_{i=1}^{i=n}\left(E_{bn}^{i}\right)^{m}} - \frac{1}{n} \cdot \sum_{i=1}^{i=n} \ln E_{bn}^{i} \qquad (20)$$

with the Weibull modulus m, the normalized breakdown strength E_{bn} and the number of tested samples n. For the first iteration step the Weibull modulus, m, calculated according to the least-squares fit method [47] was used.

The calculation of the unbiased Weibull modulus for breakdown follows equation 21

$$m_{bd} = m \cdot b(n) \qquad (21)$$

with the correction factor $b(n)$ [41] taking the number of tested samples n into account. The Weibull modulus for breakdown m_{bd} and the characteristic Weibull normalized breakdown strength, E_{0n}, with 90% CI for samples AO-R0, AO-R1, AO-R2 are summarized in table 3.

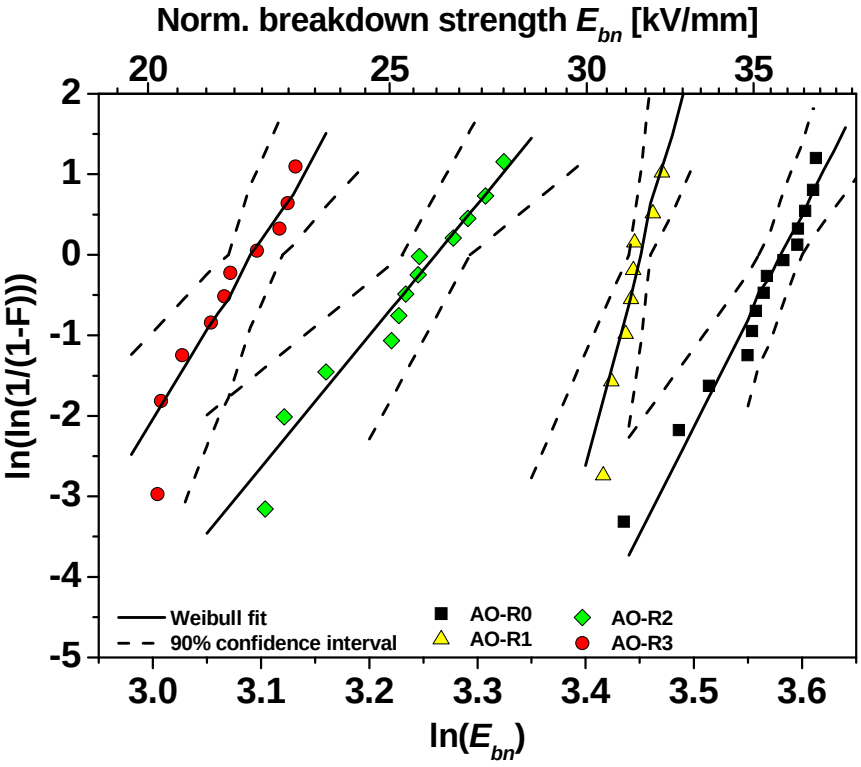

Fig. 6: Double logarithmic Weibull diagram of the failure probability as function of the normalized dielectric breakdown strength of alumina samples without rice starch AO-R0 and with rice starch as pore builder AO-R1, AO-R2 and AO-R3 (normalization thickness t = 1.0 mm). The black lines are Weibull fits and the dashed lines are 90% confidence intervals.

Table 3: Weibull moduli m_{P3B} and m_{bd} for the mechanical and breakdown test calculated according to the maximum likelihood method, characteristic Weibull strength (with 63.21% failure probability) for the mechanical and breakdown test σ_0 and E_{0n} with 90% confidence interval of AO-R0, AO-R1, AO-R2 and AO-R3.

		AO-R0	AO-R1	AO-R2	AO-R3
Fracture "P3B" test	m_{P3B}	6	5	10	13
	90%-CI of m_{P3B}	[3; 12]	[4; 9]	[7; 16]	[9; 21]
	σ_0 [MPa]	477	405	273	336
	90%-CI of σ_0 [MPa]	[425; 539]	[366; 450]	[259; 289]	[322; 351]
	Number of tested samples	6	10	10	10
Breakdown test	m_{bd}	27	51	16	22
	90%-CI of m_{bd}	[19; 39]	[31; 87]	[11; 27]	[14; 35]
	E_{0n} [kV/mm] (t=1.0 mm)	35.9	31.5	26.0	22.0
	90%-CI of E_{0n} [kV/mm]	[35.3; 36.6]	[31.2; 31.9]	[25.3; 26.9]	[21.5; 22.6]
	Number of tested samples	14	8	12	10

Weibull analysis and thickness-dependence

In figure 7, the mean breakdown strengths of alumina samples AO-R0 and AO-R2 are plotted in the range of 0.3 - 1.5 mm sample thickness. As expected from literature [5-9, 12, 18, 19, 46], the breakdown strength decreases with increasing sample thickness. The dashed lines with a slope of -0.5 indicate the "inverse square root"-dependence of the breakdown strength with respect to the sample thickness. Although the data rather exhibit a dependency of -0.4 than of -0.5 this small difference cannot be considered as significant, because 2 or 3 data points within the given error bars are not sufficient to decide between both trends. However, in our previous measurements [8] the breakdown strengths of AO-R0 are displayed in the range of 0.07 – 1.5 mm fitting a slope of -0.5 which is consistent with [6, 7, 46] for alumina. Therefore, $E_b \propto t^{-\frac{1}{2}}$ is assumed to be valid.

The highest mean breakdown strength $\overline{E}_b$ with ST.D. of 84 ± 10 kV/mm was measured for 0.3mm thick AO-R0 samples tested with DC voltage. The 1.0 mm thick AO-R0 samples, also tested with DC voltage, show $\overline{E}_b$ with ST.D. of 56 ± 4 kV/mm. In contrast to these results, $\overline{E}_b$ of samples tested with rectified AC voltage signal are found to be approximately 35 % lower.

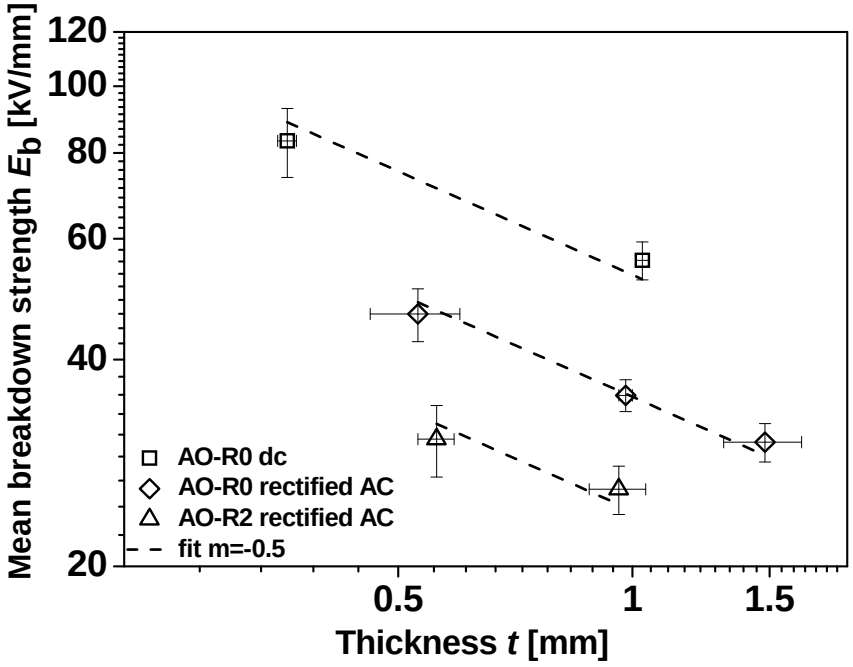

Fig. 7: Double logarithmic diagram of the mean breakdown strength, $\overline{E}_b$, with standard deviation as a function of the sample thickness, *t*, with standard deviation for alumina samples without rice starch (AO-R0) and alumina samples with 2 wt-% rice starch (AO-R2). The dashed lines are least square fits with a fixed slope of m=-0.5.

The differences in $\overline{E}_b$ due to different voltage signals are consistent with the observations of Ruemenapp et al. [10], who found 40 - 60 % lower breakdown strengths for AC tested aluminium nitride samples compared to DC tested samples.

Samples AO-R2 with 6.3 vol-% porosity show lower $\overline{E}_b$ compared to AO-R0.

The thicknesses of the samples scatter around the aspired target thicknesses which are 0.3, 0.5, 1.0 and 1.5 mm (fig. 7). Therefore, the breakdown strength values of fig. 7 were normalized with respect to the thickness to 0.3, 0.5, 1.0 or 1.5 mm according to equation 19. For samples AO-R2 the Weibull diagram is given in fig. 8.

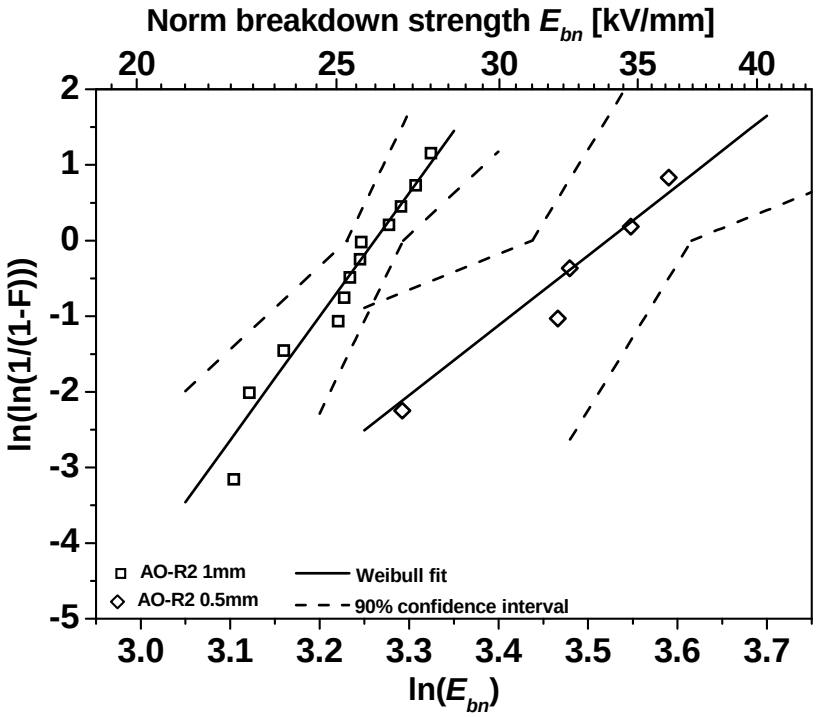

Fig. 8: Double logarithmic Weibull diagram of the normalized breakdown strength of alumina samples containing 2wt% rice starch AO-R2 for a thickness of 0.5 and 1.0 mm. The black lines are Weibull fits calculated according to the maximum likelihood method and the dashed lines are 90% confidence intervals.

Weibull moduli of $m_{bd} = 9$ and 16 were calculated according to the maximum likelihood method for samples with a thickness of 0.5 and 1.0 mm. The 90% confidence intervals and the characteristic Weibull strengths E_{0n} are given in tab. 4.

Figure 9 shows the Weibull diagram of 0.3 - 1.5 mm thick AO-R0 samples. The corresponding Weibull moduli, characteristic Weibull strengths E_{0n} and 90% confidence intervals are also summarized in tab. 4.

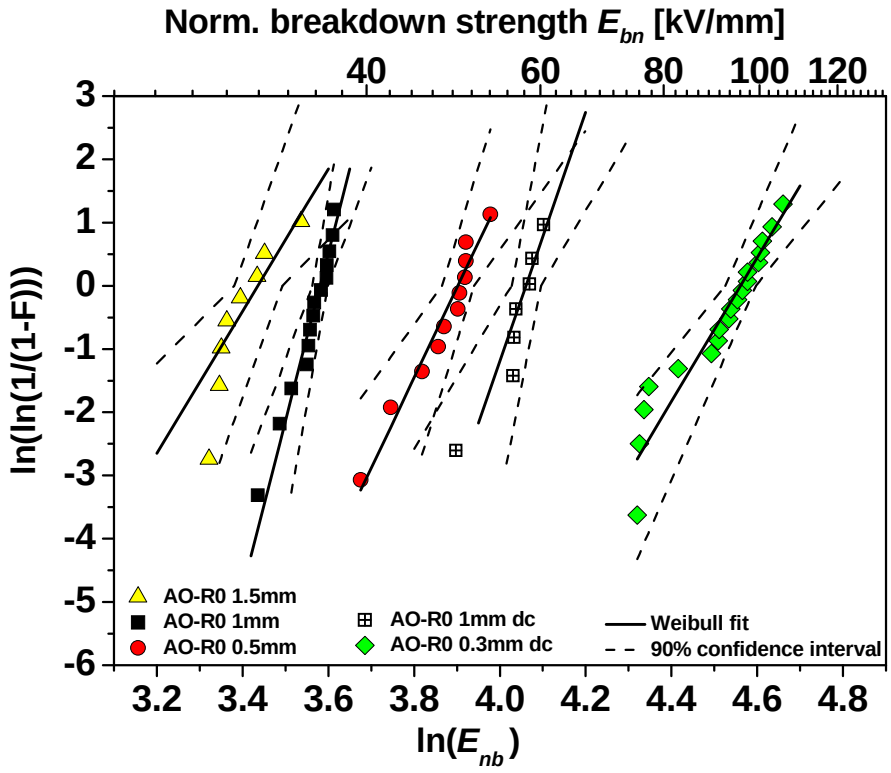

Fig. 9: Double logarithmic Weibull diagram of the normalized breakdown tests of alumina samples without rice starch (AO-R0) of different thicknesses 0.3, 0.5, 1.0 and 1.5 mm. The black lines are Weibull fits calculated according to the maximum likelihood method and the dashed lines are 90% confidence intervals.

Table 4: Weibull modulus for breakdown m_{bd}, calculated according to the maximum likelihood method and 90% confidence interval (CI), characteristic normalized Weibull strength for breakdown E_{0n} (with 63.21% failure probability) and 90%-CI.

	AO-R0					**AO-R2**	
	DC		**rectified AC**			**rectified AC**	
t [mm]	0.3	1.0	0.5	1.0	1.5	0.5	1.0
m_{bd}	11	20	14	27	11	9	16
90%-CI of m_{bd}	[8; 16]	[11; 35]	[9; 22]	[19; 39]	[7; 19]	[5; 19]	[11; 25]
E_{0n} [kV/mm]	96	58	50	36	31	34	58
90%-CI of E_{0n} [kV/mm]	[92; 99]	[56; 60]	[48; 51]	[35; 37]	[29; 33]	[31; 37]	[56; 60]
Number of tested samples	18	7	11	15	8	12	5

5. Discussion

The thickness-dependence of the breakdown strength (fig. 7) is often explained as volume-effect analogue to the mechanical case [5, 18, 19, 21-24].

In fracture mechanics, a fracture-initiating crack starts to grow from the biggest mechanically loaded defect of the sample. With increasing sample volume or thickness, respectively, the probability of failure initiating defects increases. Therefore, the fracture strength decreases with increasing sample volume or thickness, respectively [32, 33, 39, 40] (equ. 11).

If the fracture strength were plotted in a double logarithmic diagram as function of the sample volume, the slope of the curve would be $1/m$ according to equation 11. That is that same samples of different thicknesses have same Weibull moduli as experimentally shown by, e.g. Danzer et al. [32].

From the analogue expression of the failure probability for breakdown (equ. 16) the ratio of the mechanical and electrical breakdown Weibull modulus (equ. 9, 17) is expected to be constant. Furthermore, as all samples show the same thickness-dependence of the breakdown strength they all should have the same Weibull modulus, if the volume effect is assumed to be valid.

From the Weibull distribution of the mechanical P3B-test of the porous samples (fig. 3) Weibull moduli m_{P3B} of 5-13 (tab. 3) were evaluated which is in agreement to literature results [48] of P3B-tests on alumina samples.

The Weibull moduli for breakdown m_{bd} of porous alumina samples are in the range of 16-51 (tab. 3). The high m_{bd} might indicate that a chain of pores triggers the breakdown process, similar to the model of Gerson et al. [14]. But if this were the case, there should not be an effect of the surface treatment on the breakdown strength [5, 19].

The comparison of the electrical and mechanical Weibull moduli for samples AO-R2 and AO-R3 shows that their 90% confidence intervals are distinctly overlapping (tab. 3). In contrast to this finding, the mechanical and electrical Weibull moduli of samples AO-R0 and AO-R1

significantly differ from each other. For samples AO-R0 and AO-R1 the m_{P3B} with 90% CI are 6.2 [3.3; 11.7] and 5.4 [3.51; 8.58] whereas the m_{bd} with 90% CI are 26.7 [18.5; 38.6] and 51.3 [31.0; 86.9]. The mechanical and electrical Weibull moduli of samples with same porosity differ from each other but taking the 90% CI into account, a constant ratio of m_{P3B} and m_{bd} is still possible. Based on these results it is not possible to distinguish whether the volume-effect holds as explanation for the thickness-dependence of the breakdown strength.

Therefore, breakdown experiments on samples AO-R0 and AO-R2 in the thickness range of 0.3 - 1.5 mm were performed. The breakdown strength decreases as function of the sample thickness for AO-R0 and AO-R2 as shown in fig. 7. This dependence is indicated by the least-squares fit with a slope of -0.5 and is in accordance with literature results [5-9].

If the volume-effect were an explanation for the thickness-dependence of the breakdown strength, the slope of the E_b - t - curve would equal the inverse Weibull modulus. Hence, $m_{bd} = 2$ would be expected for all AO-R0 and AO-R2 samples within a thickness range from 0.3 - 1.5 mm. In contrast to this expectation the Weibull moduli for AO-R0 are in the range of 11-27, and comparable to AO-R2 with Weibull moduli in the range of 9-16 (tab. 4). Even though taking the 90% CI into account, m_{bd} significantly differs from the value 2 which were expected when the thickness-dependence of the breakdown strength were a volume-effect. As a consequence the volume-effect is no suitable explanation for the thickness-dependence of the breakdown strength. Here it should be mentioned, that no field enhancements due to edge effects or the presence of space charges were considered which might influence the absolute breakdown strength.

However, a second argument against the explanation of the thickness-dependence as volume-effect is that the thickness-dependence of the breakdown strength is also observed for ductile polymers [8]. It is highly unlikely that the mechanical fracture and the electric breakdown of a ductile material were caused by the same failure population. In contrast to brittle materials

which mechanically fail at the biggest, fracture-initiating defect, the mechanical failure of ductile materials is caused by plastic deformation.

The theoretical breakdown model developed by Schneider [49] seems to be more appropriate to explain the thickness-dependence and the scatter of the breakdown strength values. In the model it is assumed that out of a surface distribution of tiny, electrically conducting filaments the longest will start to grow, when the breakdown strength is reached. An expression for the breakdown strength [49] is given as

$$E_b = \frac{1}{c}\sqrt{\frac{6}{5\pi}}\sqrt{\frac{G_c^{bd}}{\varepsilon}}\frac{1}{\sqrt{t}}\frac{1}{\sqrt{a_c}} \qquad (22)$$

where c is a constant. Equation 22 directly shows the experimentally observed inverse-proportional relationship of breakdown strength to the sample thickness. In this model the thickness-dependence is not a consequence of the distribution of defects in the sample volume but due to the injection of space charges. Also the critical defects a_c are not identical with the defects, which cause mechanical fracture.

Talbi et al. [50] evaluated space charge limited conduction (SCLC) as dominating conduction mechanism at electric breakdown in alumina. For polymers it already has been shown that the breakdown process is associated with space charge injection, the role of the space charges is still under discussion [51]. In the case of SCLC electrons or holes are injected into the sample via the electrode. The injection process is influenced by the surface conditions of the sample, e.g. pores or a certain surface roughness could support the injection of electrons or holes into the sample due to a certain enhancement of the electric field or a disturbed band structure. This would result locally in slightly different space charge distributions. On the other hand, all filaments encounter to some extent different microstructural conditions, which can enable or hinder the growth of a filament. Both led to a fluctuation of the filament length and result in a scatter of the breakdown strength.

The failure probability for breakdown based on the breakdown model [49] is area dependent as shown in the appendix (equ. A6). This means that the failure probability should increase with increasing electrode area. Experiments by Laihonen et al. [30] on polymer films and also experiments by Block et al. [45] on alumina samples, which show a higher probability of dielectric breakdown being initiated at surface defects compared to volume defects, support this assumptions. In order to verify the area dependence of the breakdown strength for the presented model experiments on dense samples with constant thickness and varying electrode area were needed.

6. Conclusion

The breakdown strength decreases with increasing porosity of the samples and in contrast to literature results an effect of the porosity below 5 vol% on the breakdown strength is also observed.

The comparison of the Weibull moduli of the mechanical "P3B"-test, m_{P3B}, and the Weibull moduli of the breakdown test, m_{bd}, showed that the Weibull moduli significantly differ from each other. Based on the formal derivation of m_{P3B} and m_{bd}, their ratio are expected to be a constant which is within the 90% confidence intervals of m_{P3B} and m_{bd} still possible and one requirement to explain the thickness-dependence of the breakdown strength as volume-effect. As second requirement, the m_{bd} should be 2 for all samples independent of their sample thickness, which is not the case in experiment.

Therefore, the thickness-dependence of the breakdown strength cannot be explained as volume-effect.

Instead, the thickness-dependence and the scattering of the breakdown strength are explained by a theoretical breakdown model, which assumes that the breakdown process is being initiated by a distribution of conducting filaments. As the length of these filaments scatter also the breakdown strength scatter. The thickness-dependence is due to space charge injection and not a consequence of the distribution of defects in the sample volume. The critical defects, filaments in the breakdown case, are not identical with the defects, which cause mechanical fracture.

Appendix

In the breakdown model of Schneider [49] it is assumed that tiny filaments are statistically distributed at the surface of the sample with area A. In order to describe the failure probability for breakdown the same approach can be used as in the mechanical case but for surface defects [20, 40]. The failure probability for dielectric breakdown is:

$$P_f^{bd} = 1 - \exp\left[-N_c^{bd}(E_b, A)\right] \qquad \text{(A1)}$$

with N_c^{bd} the number of critical filaments in the area A and the critical breakdown strength E_b. If the size distribution frequency of critical surface filaments is:

$$g_A(a) = \frac{l-1}{A_0 a_0}\left(\frac{a}{a_0}\right)^{-l}, \quad (l > 1) \qquad \text{(A2)}$$

where l is a constant, A_0 is a normalization area, and a_0 a normalization filament length. The mean number of critical filaments for dielectric breakdown is:

$$N_c^{bd}(a_c, A) = A\int_{a_c}^{\infty} g_A(a)da = \frac{A}{A_0}\left(\frac{a_c}{a_0}\right)^{1-l} \qquad \text{(A3)}$$

with the energy release for breakdown from the theoretical breakdown model [47]:

$$G_{bd} = c^2 \frac{5\pi}{6} E_b^2 \, \varepsilon \, a_c t \qquad \text{(A4)}$$

with a constant c, the permittivity ε, the thickness t and the critical filament length a_c and the dielectric breakdown criterion (11) it follows:

$$N_c^{bd}(E_b, A) = \frac{A}{A_0}\left(\frac{\frac{1}{E_b^2}}{\frac{1}{E_0^2}}\right)^{1-l} = \frac{A}{A_0}\left(\frac{E_b}{E_0}\right)^{2(l-1)} \qquad \text{(A5)}$$

Introducing (A5) into (A1) gives:

$$P_f^{bd} = 1 - \exp\left[-\frac{A}{A_0}\left(\frac{E_b}{E_0}\right)^{m_{bd}}\right] \qquad \text{(A6)}$$

with the Weibull modulus for dielectric breakdown:

$$m_{bd} = 2(I - 1) \qquad \text{(A7)}$$

This result predicts that the failure probability for breakdown should increase with increasing electrode area.

Acknowledgements

The authors gratefully acknowledge the financial support by the German Research Foundation (DFG) under Project number SCHN-372/17-1. We thank Jean-Marc Pasquire for his help in sample preparation and characterization.

References

[1] Blais, G., Le Gressus, C. Charging and flashover induced by surface polarization relaxation process. J. Appl. Phys., 1991;69:6334 – 6339.

[2] Liebault J., Vallayer D., Goeuriot D., Treheux D., Thevenot F. How the trapping can explain the dielectric breakdown performance of alumina ceramics. J Eur. Ceram. Soc., 2001;21:389 – 397.

[3] Touzin M., Goeuriot D., Guerret-Piécourt C., Juvé D., Fitting H.-J. Alumina based ceramics for high-voltage insulation. J Eur. Ceram. Soc., 2010;30:805 – 817.

[4] Touzin M., Goeuriot D., Fitting H.-J., Guerret-Piécourt C., Juvé D., Tréheux D. Relationships between dielectric breakdown resistance and charge transport in alumina materials-Effect of the microstructure. J Eur. Ceram. Soc., 2007;27:1193 – 1197.

[5] Owate, I.O., Freer, R., The electrical properties of some cordierite glass ceramics in the system MgO-Al_2O_3-SiO_2-TiO_2. J. Mater. Sci., 1990:25;5291-5297.

[6] D. Malec, V. Bley, F. Talbi, F. Lalam, Contribution to the under-standing of the relationship between mechanical and dielectric strengths of Alumina. J. Eur. Ceram. Soc., 2010;30:3117–3123.

[7] Talbi, F., Lalam, F., Malec, D., Dielectric Breakdown Characteristics of Alumina. IEEE, International Conference on Solid Dielectrics, 2010;1 – 4.

[8] Neusel C., Schneider G. A., Size-dependence of the dielectric breakdown strength from nano- to millimeter scale. J. Mech. Phys. Solids. 2014:63;201–213.

[9] Neusel C., Schneider G. A., Size and permittivity dependence in the breakdown strength. IEEE Proceeding of the Conference of Solid Dielectrics ICSD 2013, 31–35.

[10] Ruemenapp T., Peier D., Dielectric breakdown in aluminum nitride. High Voltage Engineering Symposium, 1999;467:22-27.

[11] Malec, D., Bley, V., Lebey. T., Talbi, F., Lalam, F., Investigation on Dielectric Breakdown of Ceramic Materials. IEEE, Annual Report Conference on Electric Insulation and Dielectric Phenomena, 2005, 63-66.

[12] Chen G., Zhao J., Li S., Zhong L., Origin of thickness dependent DC electrical breakdown in dielectrics. Appl. Phys. Lett. 2012;100: 222904-1 - 222904-4.

[13] Beauchamp E. K., Effect of microstructure on pulse electric strength on MgO. J. Am, Ceram. Soc. 1971;54:484-487.

[14] Gerson, R., Marshall, T. C., Dielectric Breakdown of Porous Ceramics. J. Appl. Phys. 1959;30:1650-1653.

[15] Haddour, L., Mesrati, N., Goeuriot, D., Tréheux, D., Relationship between microstructure, mechanical and dielectric properties of different alumina materials. J. Eur. Ceram. Soc. 2009;29:2747 – 2756.

[16] Si Ahmed A., Kansy J., Zarbout K., Moya G., Liebault J., Goeuriot D. Microstructural origin of the dielectric breakdown strength in alumina: A study by positron lifetime spectroscopy. J. Eur. Ceram. Soc. 2005;25:2813 – 2816.

[17] Tunkasiri, T., Rujijanagul, G., Dielectric strength of fine grained barium titanate ceramics. J. Mater. Sci. Lett. 1996:15;1767-1769.

[18] Owate, I.O., Freer, R., Dielectric breakdown of ceramics and glass ceramics. Sixth International Conference on Dielectric Materials, Measurements and Applications 1992, p. 443-446.

[19] Owate, I.O., Freer, R., The AC Electrical Breakdown of Some Aluminum Nitride Ceramics. Silicates Industriels, 1989:7-8;123-127.

[20] Munz, D., Fett, T., Ceramics Mechanical Properties, Failure Behaviour, Materials Section. In: Hull, R., Osgood Jr., R. M., Sakaki, H., Zunger, A. editors, Springer Series in Material Science 36. Springer-Verlag Berlin; 2001.

[21] Nakamura Y., Suzuki M., Motohira N., Kishimoto A., Yanagida H., Comparison between the mechanical and dielectric strength distributions for hardened gypsum. J. Mater. Sci. 1997;32:115-118.

[22] Yamyshita K., Koumoto K., Yanagida H., Hamano T., Analogy between mechanical and dielectric strength distribution for $BaTiO_3$ ceramics. Communication of the American Ceramic Society 1984, C-31 – C-33.

[23] Kishimoto A., Koumoto K., Yanagida H., Mechanical and dielectric failure of $BaTiO_3$ ceramics. J. Mater. Sci. 1989, 698 – 702.

[24] Kishimoto A., Koumoto K., Yanagida H., Comparison of mechanical and dielectric strength distribution for various surface-finished titanium dioxide ceramics. J. Am. Ceram. Soc. 1989;72:1373 – 1376.

[25] Young A. L., Hilmas G. E., Zhang S. C., Schwartz R. W., Mechanical vs. electrical failure mechanisms in high voltage, high energy density multilayer ceramic capacitors. J. Mater. Sci. 2007;42:5613 – 5619.

[26] Stark H. K., Gorton C. G., Electric strength of irradiated polythene. Nature, 1955;176:1225 – 1226.

[27] Zeller H. R., Schneider W. R., Electro fracture mechanics of dielectric aging. J. Appl. Phys. 1984;56:455-459.

[28] Fothergill, J.C., Filamentary Electromechanical Breakdown. IEEE Transactions on Electrical Insulation, 1991:26;1124-1129.

[29] Carbajar C., Olangnon C. Fantozzi G., Le Gressus C., Relations between electrical breakdown field and mechanical properties of ceramics. Annual Report Conference in electrical insulation and dielectric phenomena, 1995;278 – 281.

[30] Laihonen S. J., Gäfert U., Schütte T., Gedde U.W., DC breakdown strength of polypropylene films: area dependence and statistical behavior. IEEE Transactions on Dielectrics and Electrical Insulation 2007:14; 275-286.

[31] Cygan, S., Laghari, J.R., Dependence of the electric strength on thickness area and volume of polypropylene. IEEE Transactions on Electrical Insulation 1987:6;835-837.

[32] Danzer R., Börger A., Supancic R., Ruiz Villanueva M. A., Ein einfacher Festigkeitsversuch für Scheiben aus spröden Werkstoffen. Mat.-wiss. Und Werkstofftech. 2003:34;490-498.

[33] Danzer, R., Harrer, W., Supancic, P., Lube, T., Wang, Z., Börger, A., The ball on three balls test – Strength and failure analysis of different materials. J. Eur. Ceram. Soc. 2007:27;1481-1485.

[34] Neusel C., Jelitto H., Schmidt D., Janssen R., Felten F., Schneider G.A., 2012. Dielectric breakdown of alumina single crystals. J. Eur. Ceram. Soc. 2012:32;1053–1057.

[35] Börger, A., Supancic, P., Danzer, R., The ball on three balls test for strength testing of brittle discs: stress distribution in the disc. J. Eur. Ceram. Soc. 2002:22;1425-1436.

[36] Freudenthal, A. M., Statistical approach to brittle fracture. In: Liebowitz, H., editor. Fracture, An Advanced Treatise Vol.2 Mathematical Fundamentals. Academic Press new York; 1968, p. 592-619.

[37] Gross, D., Seelig, Th., Bruchmechanik - Mit einer Einführung in die Mikromechanik. 5. Auflage Berlin: Springer-Verlag; 2011.

[38] Jayatilaka, A. de S., Trustrum, K., Statistical approach to brittle fracture. J. Mater. Sci. 1977:12;1426 – 1430.

[39] Danzer, R., A general strength distribution function for brittle materials. J. Eur. Ceram. Soc. 1992:10;467-472.

[40] Danzer, R., Lube, T., Supancic, P. and Damani, R., Fracture of Ceramics. Adv. Eng. Mater. 2008:10;275–298.

[41] DIN EN 843-5 Advanced technical ceramics – Mechanical properties of monolithic ceramics at room temperature – Part 5: Statistical analysis; German version EN 834-5:2006.

[42] Coble, R. L., Kingery, W. D., Effect of porosity on physical properties of sintered alumina. J. Am. Ceram. Soc. 1956:39;377-385.

[43] Knudsen, F. P., Dependence of mechanical strength of brittle polycrystalline specimens on porosity and grain size. J. Am. Ceram. Soc. 1959:42;376-387.

[44] ASTM Standard D 149-97a, Standard test method for Dielectric Breakdown Voltage and Dielectric Strength of Solid Electrical Insulating Materials, 2007.

[45] Block B., Kim Y., Shetty D.K., Dielectric breakdown of polycrystalline alumina: A weakest-link failure analysis. J. Am. Ceram. Soc. 2013:96;3430-3439.

[46] Forlani, F., Mannaja, N., Electrical Breakdown in Thin Dielectric Films. J. Vac. Sci. Technol. 1969:6;518-526.

[47] Fahrmeir, L., Künstler, R., Pigeot, I., Tutz, G., Statistik. 6. Auflage Berlin: Springer-Verlag; 2006.

[48] Seidel, J., Claussen, N., Rödel, J., Reliability of alumina ceramics. 2: Effect of processing. J. Eur. Ceram. Soc. 1997:17;727-733.

[49] Schneider, G.A., A Griffith type energy release rate model for dielectric breakdown under space charge limited conductivity. J. Mech. Phys. Solids. 2013:61;78–90.

[50] Talbi, F., Lalam, F., Malec, D., DC conduction of Al_2O_3 under high electric field. J. Phys. D: Appl. Phys. 2007:40;3803–3806.

[51] Blaise, G., Space-charge physics and the breakdown process. J. Appl. Phys. 1995:77,2916-2927.